HIGH CURRENT LINAC DESIGN WITH EXAMPLES OF RESONANCES AND HALO

F. Gerigk, CLRC, RAL, Chilton, UK

K. Bongardt, FZ Jülich, Germany, I. Hofmann, GSI, Darmstadt, Germany

Abstract

The next generation of proton drivers that are now under study in various laboratories, or already under construction, have to transport high intensity beams while keeping the losses below the margin of 1 W/m. In preparation for these machines a considerable amount of theoretical work has been published, aimed at understanding the dynamics of halo development and emittance growth. In this paper we review some of this work and apply the findings to a realistic machine design. Our goal is to present recipes for a high current linac design and to understand how the machine design can influence the development of halo and emittance growth in case of mismatch.

1 INTRODUCTION

All present studies (see i.e. [1], [2], [3], [4]) for high current linac designs are based on a beam loss limit of 1 W/m, a value that stems from the experience of LANSCE [5] and which is meant to ensure hands-on-maintenance. With beam powers ranging between 1 and 10 MW this figure transforms into a maximum beam loss per metre of the order of 10^{-6} to 10^{-7}. Although the experience with LAN-
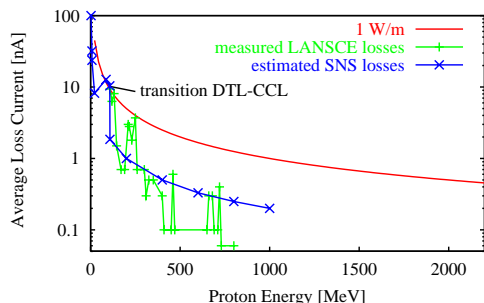

Figure 1: Beam loss budget for 1 W/m, measured losses from LANSCE, estimated losses for the SNS [6], [7].

SCE (Fig. 1) seems to encourage the design of low-loss linacs, it has to be pointed out that its maximum output power of 1 MW was only achieved with proton beams, which neither suffer from residual gas H^- stripping [8] nor from the generally less favorable output distribution of existing H^- sources. Furthermore, all new linac designs rely on H^- charge-exchange injection into subsequent accelerators or accumulator and compressor rings, which poses additional constraints on beam quality, in comparison to the LANSCE - PSR machines.

To resolve beam losses of the order of 10^{-7}, the simulation tools either have to track particle numbers exceeding 10^7, which can be achieved with parallelized codes like IMPACT [9]. Alternatively, it is proposed to combine results from many runs using lower numbers of particles, an approach used in TRACE_WIN [10]. In Fig. 2 we show transverse particle distributions for 10^5, 10^6, and 10^7 particles from IMPACT simulations of the CERN SPL [11] with a strongly mismatched Gaussian input distribution. Although the maximum radius is almost identical for all
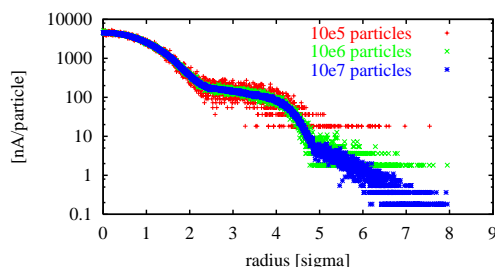

Figure 2: Transverse particle distribution sampled from CERN SPL simulations with 10^5, 10^6, and 10^7 particles.

three simulations, a precise loss prediction clearly benefits from simulations with 10^7 particles.

This paper is organized in the following way: we first review the mechanics of halo development and r.m.s. emittance growth and then use the findings to minimize losses in an actual machine design.

2 HALO DEVELOPMENT

Using the parametric resonance model [12] one can easily understand single particle effects by looking at the integer ratio between single particle tunes and: a) the periodicity of the lattice, or b) the envelope oscillation of an r.m.s. mismatched beam core around its matched equilibrium. Due to the strong tune depression in high intensity linacs (usually $(\sigma/\sigma_0) > 0.5$) there is a large spread of single particle tunes $\sigma \leq \sigma_p \leq \sigma_0$ which are prone to parametric resonances.

Lattice resonances are usually avoided by keeping the zero current tunes per period (and therefore all single particle tunes σ_p) below 90°, leaving the particle-core resonances as the major cause for halo development. The integer ratio (mostly 2:1) between the single particle tunes and the envelope tunes of the core oscillations allows energy transfer from the core movement to the single particle orbits [12]. Thus, the "free energy" which is introduced into the system via mismatch is transformed into emittance growth and halo development until the r.m.s. beam core settles again on a matched orbit. Due to the large spread of single particle

tunes, this mechanism is the major source of beam halo in high-intensity linacs.

To study parametric resonances systematically, one can derive the three eigenmodes of a 3D bunched beam and excite them by a specific initial mismatch [13] using equal variations for the Twiss parameters α and β per plane. With this approach the modes can be excited at any location in the lattice with their maximum amplitude. The resulting oscillations of the core around its equilibrium state are stable as long as the envelope frequencies of the modes remain below 180° and may remain remarkably stable throughout a full linac, although the tunes usually change substantially [1]. All simulations in the following use a gaussian input distribution, since the transformation of mismatch into beam halo tends to be much faster than for a waterbag distribution [19].

2.1 Initial Mismatch & Beam Halo

In order to study the redistribution of particles in cases of mismatch, we consider fixed points around which halo particles conglomerate. Their distance from the core is determined by the 2:1 parametric tune ratio and is therefore given by the oscillation frequency of the core. Fig. 3 shows the envelope frequencies of the three eigenmodes for the superconducting part of the SPL.
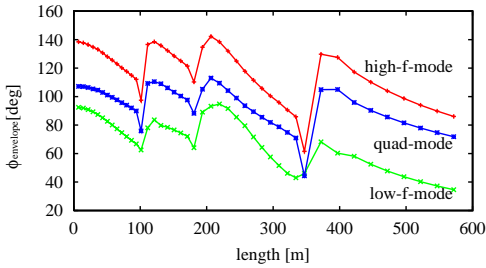

Figure 3: Envelope frequencies of the three eigenmodes for the superconducting part of the SPL.

Although the fixed point core distance can theoretically go to infinite values one observes that the maximum halo radii found in simulations are limited to a certain threshold (see next section). Ref. [14] suggests that for increasing fixed point core distances there is a decrease in the space charge coupling force, which is responsible for the energy transfer from the core oscillations to the single particle oscillations. As a result, fixed points with increasing core distances get less and less populated.

In Fig. 4 we plot the transverse redistribution of particles due to eigenmode excitation in the SPL. We can see that the quadrupolar mode, which only oscillates in the transverse plane, displaces particles from the core $0 < r \le 1\sigma$ to orbits around $\approx 2\sigma$, which is easy to understand since it oscillates about twice as fast as the core particles in transverse phase space. For the high- and low-frequency mode the situation is more complicated as we can excite radial
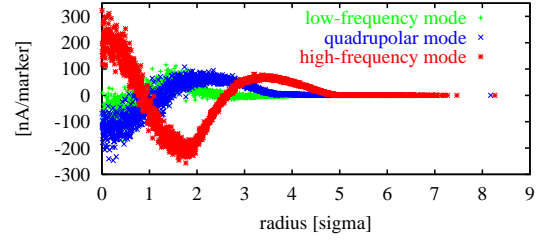

Figure 4: Transverse particle redistributions for a Gaussian beam with 30% eigenmode excitation (maximum matched radius: $\approx 4 - 5\sigma$); plotted is the difference in distribution with respect to the output beam of the matched case.

and axial oscillations and because the particles have different tunes in transverse and longitudinal phase space. Additionally, the redistribution gets mixed with oscillations from the phase slippage in the superconducting cavities of the simulated lattice. Nevertheless, the redistribution pattern in Fig. 4 is consistent with the fixed point model: the frequency of the low-frequency mode is below that of the quadrupolar mode which means that it can only develop a very weakly coupled 2:1 resonance to the core particles, which have the lowest (depressed) tune values. As a result, the low-frequency mode redistributes very few particles and develops a fixed point at a smaller core distance than the quadrupolar mode. The high-frequency mode couples to bunch particles with higher tunes, which are located further away from the core between 1 and $2\,\sigma$ and displaces them surprisingly not only around a fixed point at $\approx 3.5\sigma$ but also towards the beam centre. We assign this effect to the non-linear high-frequency flutter which is created by phase slippage.

Using a general +++ mismatch[2] we find the redistribution pattern shown in Fig. 5. Decomposing the +++ excitation in
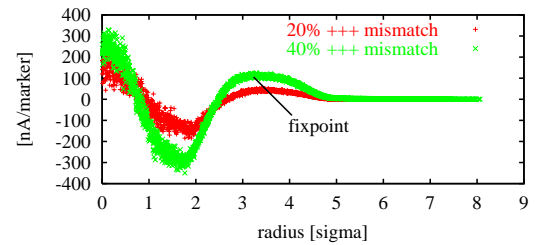

Figure 5: Transverse particle redistribution for a Gaussian beam with 20% and 40% initial +++ mismatch.

eigenmodes one finds that the transverse excitation amplitude for the high-frequency mode in this case is ≈ 6 times higher than for the low-frequency mode, while the longitudinal excitation amplitudes are approximately equal[3]. Accordingly, one can see that the transverse redistribution pattern for the +++ mismatch is completely dominated by the high-frequency mode pattern.

---

[1] which corresponds to keeping the zero current tunes below 90°

[2] a mismatch with: $\frac{\Delta r_{x0}}{r_{x0}} = \frac{\Delta r_{y0}}{r_{y0}} = \frac{\Delta r_{z0}}{r_{z0}}$

[3] due to equal excitation in x and y the quadrupolar mode is not excited

Since the location of fixed points depends not only on the type of initial mismatch but also on the tunes in the different planes, the tune ratio ($k_{long}/k_{transv.}$) [14] and the beam emittances, it is difficult to provide a general prediction of the particle redistribution pattern in an actual design. We therefore suggest using either all three eigenmodes to examine halo development or at least different types of initial mismatch like +++, +-+[4], etc. (see Fig. 6).
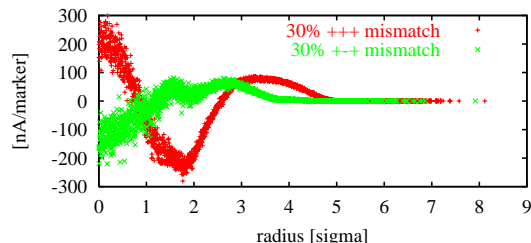

Figure 6: Transverse particle redistribution for 30% initial +++/+-+ mismatch in the SC section of the SPL.

2.2 Extent of Transverse Halo

In the previous section we found that the probability of particles populating halo fixed points decreases with increasing core distances. Using a high number of particles (10^7) for a Gaussian input beam we find in Fig. 7 that the maximum transverse particle radius remains almost constant, when we use the same kind of initial mismatch (+++) with different amplitudes. One can observe that the redistribu-
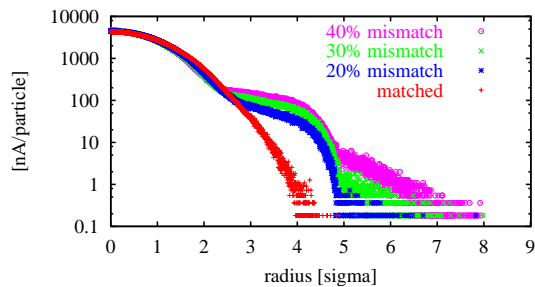

Figure 7: Transverse particle distribution for initial +++ mismatch in the SC section of the SPL.

tion pattern remains the same and that only the number of particles that are displaced to different areas of the bunch increases. This confirms the idea that the extent of halo due to initial mismatch is limited [15], with the maximum radius, in our case, being at about 8 times the matched r.m.s. radius. Nevertheless, due to lattice transitions we find locally higher radii especially in the low energy part of the SPL, where particles reach up to 11σ for a 40% initial mismatch (Fig. 8). A practical design suggestion would be to use a safety margin of $\approx 11\sigma$ in the quadrupoles, where the beam radius reaches its maximum.
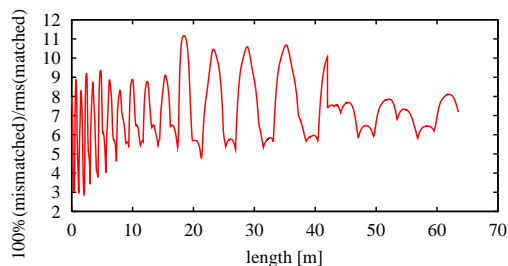

Figure 8: 100% over (matched) r.m.s. radius for a normal conducting linac with lattice transition at 17 and 43 mm, 40% +++ initial mismatch excitation.

2.3 Mismatch due to Distributed Errors

While the study of initial mismatch defines the limits for the matching between different sections of the linac and also provides us with an estimate for the maximum halo extent, the study of distributed mismatch eventually defines the tolerances of each element. The outcome of simulations with statistically distributed alignment and field errors is different for each machine and sets the limits for mechanical precision and the quality of the RF. Although larger bore radii yield higher RF power consumption and require magnets with higher pole tip fields the benefits of increased alignment tolerances and reduced beam loss can easily outweigh this price.

3 CORE EFFECTS

Single particle resonances eventually yield r.m.s. emittance growth as more and more particles get trapped in new large amplitude orbits. However, this redistribution is not caused by a "collective" effect involving all core particles but is triggered by mismatch. Real core - core resonances are observed for non-equipartitioned r.m.s. matched beams fulfilling internal resonance conditions between the planes. Assuming a linac beam which is usually equipartitioned in x and y ($T_{xy} = \frac{\varepsilon_x k_x}{\varepsilon_y k_y} = 1$) but has different "beam temperatures" in the longitudinal and transverse plane ($T_{xz} \neq 1$), the core resonances enable "energy transfer" from the hotter to the colder plane until the beam moves out of the unstable area towards equipartition. The self consistent theory was derived in 2D [16], confirmed with 3D simulations for a constant focusing channel [17], and then validated with several test lattices using two sections of the SPL [18]. Fig. 9 shows a stability chart, derived for the SPL emittance ratio $\varepsilon_l/\varepsilon_t = 2$ with the tune footprints of three lattices that merely differ by their quadrupole settings. The dominant 4th order resonance at $k_z/k_x = 1$, which proves to be most harmful, yields significant emittance exchange for case 2 but an undisturbed emittance evolution for the two other cases [18] (Fig. 10). We note that the exchange is not accompanied by halo creation and that in the presented case one "hot" plane is feeding two "cold" planes.

This result gives a clear indication that equipartitioning is not a necessary feature in the design of high intensity

---

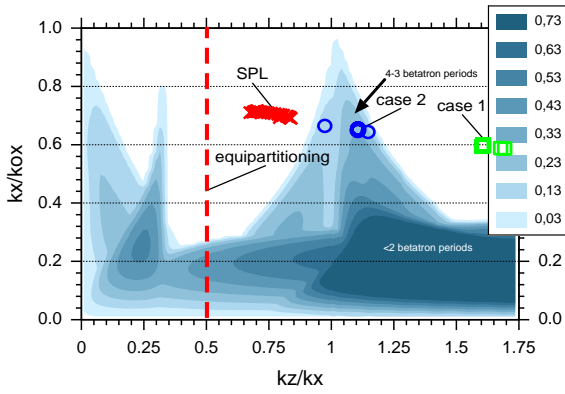[4]which excites, contrary to +++, all three eigenmodes at the same time

Figure 9: Stability chart for $\varepsilon_l/\varepsilon_t = 2$ with the SPL reference tunes between 120 and 390 MeV, and two cases with modified quadrupole settings.

linacs and that even pronounced anisotropic beams (case 1: $T_{xz} \approx 3.2$) can be transported.
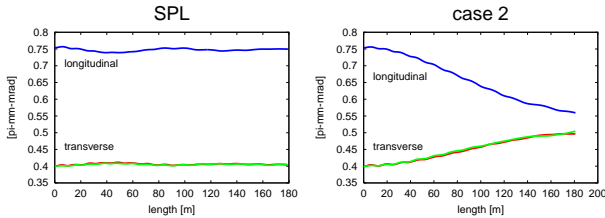

Figure 10: R.m.s. emittance evolution for the SPL reference lattice and case 2.

A recent study [19] showed that the r.m.s. emittance growth rates in the different planes due to initial mismatch also depend on the ratio of the full current tunes. While the emittance growth in the transverse and longitudinal planes can be different it turned out that the averaged r.m.s. emittance growth[5] is almost constant. This also supports the "free energy" concept.

4   LINAC DESIGN

4.1   Focusing Length

One of the starting points in every linac design is the length of the focusing periods. Since the electric field gradient is usually a fixed value, being determined by maximum surface fields, RF windows, power couplers, power supplies, RF frequency, etc., the choice of focusing length is basically a choice of the longitudinal and transverse tunes per period. In normal conducting structures, the small bore radii in the cavities demand strong transverse focusing. In order to avoid emittance exchange one would therefore choose a working point in the stability chart (see Fig. 9) with $k_z/k_x < 1$, e.g. ≈ 0.8, which means in this case the period length is determined by the maximum transverse

---

[5] $(\Delta\varepsilon_x/\varepsilon_x + \Delta\varepsilon_y/\varepsilon_y + \Delta\varepsilon_z/\varepsilon_z)/3$

tune, which has to be kept safely below 90° for all particles. In a superconducting linac where the risk of transverse beam loss is very low due to the large bore and tube radii, one is free to choose a working point with tune ratios > 1 (see case 1 in Fig. 9), on the right side of the stop band. In this case the design is dominated by the maximum longitudinal tune ($\sigma_{l0} < 90^o$).

If the required transverse focusing strength in a DTL cannot be achieved due to the restricted quadrupole space inside the drift tubes one can use FFDD [20], FFODDO [21], or even FFFDDD focusing to use the given quadrupole strength more effectively. In SC linac sections one often uses quadrupole doublets (FDO) to provide long drifts to accommodate the cryostats.

4.2   Lattice Transitions & Emittance Growth

In order to treat this subject we designed three different normal conducting linacs that accelerate a 40 mA beam from 3 to 120 MeV. The parameters of each linac meet the SPL requirements (see also [20]). Linac No. 1 uses 9 Alvarez drift tube linac (DTL) tanks, which are spaced by a "missing gap", meaning that there are 8 longitudinal transitions to be matched. Linac No. 2 uses three DTL tanks and 37 coupled cavity drift tube linac (CCDTL) tanks with three or four gaps per tank. In this linac we have two longitudinal transitions (between the DTL tanks), one transition in both planes (DTL/CCDTL), and one transverse transition between the 3-gap and the 4-gap CCDTL lattice. For Linac No. 3 we choose a lattice without any transition reusing the lattice of Linac 1 with the assumption that we can omit the "missing gaps" between the DTL tanks. From Fig. 11 we can see that Linac 1, the version with the highest number of longitudinal transitions, shows the largest longitudinal emittance growth. Transversely, the growth pattern
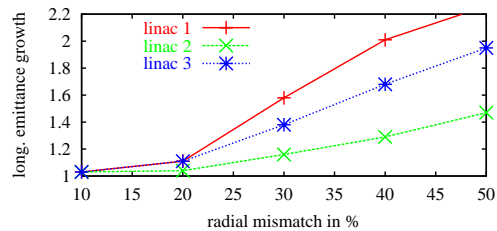

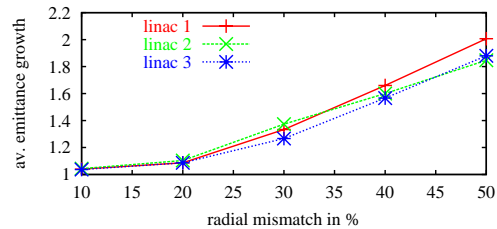Figure 11: Longitudinal r.m.s. emittance growth for three test linacs with initial +++ mismatch.

Figure 12: Averaged r.m.s. emittance growth for three test linacs with initial +++ mismatch.

is reverse and we find that Linac 1 has the lowest transverse emittance growth, while Linac 2 exhibits the largest transverse growth rate. Looking at the averaged emittance growth rates in Fig. 12 we find that even the transitionless Linac 3 has the same averaged emittance growth as the two other versions. This means that, as long as the transitions between different linac sections are properly matched, keeping the phase advance per metre as smooth as possible, the lattice choice can influence the plane in which the major emittance growth takes place but clearly does not influence the averaged emittance growth. Nevertheless we should keep in mind that matching transitions in a simulation is quite different from the situation in real life, therefore we recommend using as few transitions as possible.

4.3 Measures to Limit Beam Loss

In section 2 we saw that even for strong mismatch the transverse beam radius remains limited and that apertures of $\approx 11\sigma$ seem to be a sensible design choice.

In a normal conducting linac one attempts to keep the apertures as small as possible to reduce RF power consumption. In the low energy part of a DTL an additional limit for the aperture is given by the length over aperture ratio of the quadrupoles, which determines the quadrupolar field quality. In case of a DTL the only option to reduce losses is to apply beam scrapers, preferably before the DTL tanks. By separating magnets and RF, as done in a CCDTL or a coupled cavity linac (CCL), one can raise the quadrupole aperture without lowering the RF efficiency. Using the example of the normal conducting linac No. 2 from section 4.2, we introduce an initial +++ mismatch and obtain the loss pattern depicted in Fig. 13. The losses occur on 4 "hot
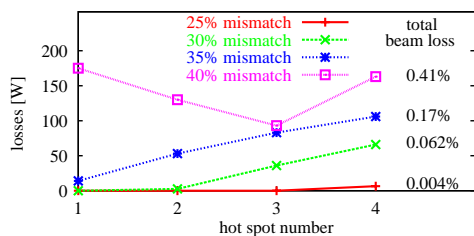

Figure 13: Losses at four hot spots in the CCDTL part of the SPL normal conducting linac with a continuous beam pipe radius of $\approx 7\sigma$.

spots" in the CCDTL, which was designed with a tube over r.m.s. beam size ratio of ≈ 7. Using a scraper at the beginning of the DTL, which cuts off high amplitude particles ($\approx 0.003\%$ of the beam), and raising the quadrupole aperture radius from 16 to 25 mm ($\approx 11\sigma$), the losses of the 40% mismatch case could be reduced to a total of 0.62 W distributed on two spots! If the quadrupole aperture has to be kept smaller we propose using a thin carbon layer, which can help to reduce the activation by lost particles.

5 CONCLUSIONS

Emittance growth and halo development in high-intensity linacs is primarily caused by mismatch, resulting from badly matched input beams, transitions between sections, or more generally: rapidly changing lattice functions, misaligned elements, and field & gradient errors. Parametric resonances between single particles and the oscillations of a mismatched beam core explain the migration of particles to large amplitude orbits. The parametric 2:1 tune ratio also defines the position of fixed points, which attract the halo particles. However, with increasing core distance the fixed points get less populated, eventually yielding a limitation for the maximum halo radius. We suggest a safety margin of $\approx 11\sigma$ in the quadrupoles to avoid losses. The knowledge of core resonances and the resulting stability plots may be used to avoid emittance exchange between the planes. We also find that the number and type (longitudinal/transverse) of lattice transitions determines the partitioning of emittance growth in the three planes but does not influence the averaged emittance growth. In an actual high-intensity linac design we suggest the use of scrapers before entering DTL tanks, and if possible to separate the quadrupoles from the RF structure to provide enough design freedom to reduce transverse losses in normal conducting structures without lowering the RF efficiency.

6 ACKNOWLEDGMENTS

7 REFERENCES

[1] J. Wei, M. Blaskiewiez, et. al., *PAC01*

[2] J. Stovall et. al., *PAC01*

[3] K. Bongardt, M. Pabst, *EPAC96*

[4] A. Mosnier, *this conference*

[5] http://lansce.lanl.gov

[6] N. Catalan-Lasheras (Ed.), *SNS/AP Technical Note 07*

[7] S. Schriber, NC/SC proton linacs, seminar, CERN 11/01

[8] The ESS Project, Technical Report, Vol.3
http://essnts.ess.kfa-juelich.de/TheEssProject

[9] J. Qiang et.al. , *J. of Comp.Ph., 163, 434*, 9/2000

[10] N. Pichoff, D. Uriot, *DSM/DAPNIA/CEA 2000/45*

[11] M. Vretenar (Ed.), *CERN 2000-012*

[12] Gluckstern, *Ph.Rev.Letters 73*, 1247

[13] A. Letchford et.al. , *PAC99*

[14] G. Franchetti et.al. , *Ph.Rev. Letters, 88, 254802*

[15] T. Wangler, *ICAP98*

[16] I. Hofmann, *Physical Review E, Vol. 57/4*, 1998

[17] I. Hofmann et.al. , *Ph.Rev. Letters 86*, 2313

[18] F. Gerigk, I. Hofmann, *PAC01*

[19] I. Hofmann et.al. , *EPAC02*

[20] F. Gerigk, M. Vretenar, *this conference*

[21] J. Billen et.al. , *PAC01*